A combined regional Geopotential Model using optimized global Gravity Field Solutions

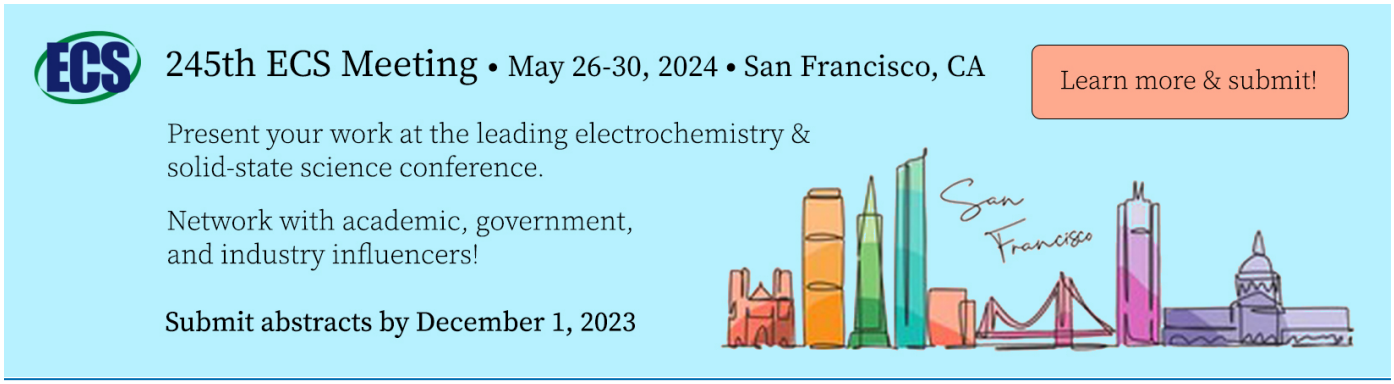

A combined regional Geopotential Model using optimized global Gravity Field Solutions

C J Nyoka[1], A H M Din[1,2], M F Pa'suya[3] and A H Omar[4]

[1] Geospatial Imaging and Information Research Group (GI2RG), Faculty of Built Environment and Surveying, Universiti Teknologi Malaysia, 81310 Skudai, Johor, Malaysia.
[2] Geoscience and Digital Earth Centre (INSTeG), Faculty of Built Environment and Surveying, Universiti Teknologi Malaysia, 81310 Skudai, Johor, Malaysia.
[3] Environment and Climate Change Research Group (ECCG) Faculty of Architecture, Planning & Surveying, Universiti Teknologi MARA, Perlis, Arau Campus, 02600 Arau, Perlis, Malaysia
[4] Geomatics Innovation Research Group (GnG), Faculty of Built Environment and Surveying, Universiti Teknologi Malaysia, 81310 Skudai, Johor, Malaysia.

E-mail: jnchivatsi@graduate.utm.my; amihassan@utm.my

Abstract. To develop a gravimetric geoid, a Global Geopotential Model (GGM) is required to minimise the truncation error arising from using the Stokes integral with a limited number of gravity data points. The choice of a best-fitting GGM determines the accuracy of a gravimetric geoid solution. Selecting a suitable GGM is a rigorous process, requiring both internal and external evaluation of all GGMs available at the International Center for Globa Earth Models (ICGEM). Moreover, GGMs perform differently depending on the wavelength, and it is difficult to obtain a GGM that performs best across the full harmonic spectrum. In this study, a combined GGM is developed from a selection of the most recent and high-resolution GGMs covering Peninsular Malaysia. The selected models are first synthesized harmonically to obtain geoid undulations at collocated GNSS-levelled points, and free air anomalies at randomly sampled points across the study area. These quantities are compared with the observed geoid undulations and point gravity anomalies interpolated from a grid of free air anomalies. The best performing GGMs are then used to produce a combined GGM, by selecting the spherical harmonic coefficients with the best characteristics for every degree. The signal and error spectra of the new GGM are compared with the selected geopotential models. The combined GGM produced a higher cumulative signal to noise ratio (SNR) of 4402.669 compared to all the selected GGMs, with XGM2016 and Eigen-6C following suit with SNR of 4139.561 and 4092.462, respectively. Besides, the new combined GGM performed better across the whole harmonic spectrum than all selected GGMs. The use of combined GGMs in geoid modelling, instead of a single GGM may be more desirable because they can improve the quality of results.

1. Introduction

The Stokes integral formula is widely used to create a gravimetric geoid model, by computing geoidal undulations using gravity measurements at places on the earth's surface This formula requires gravity data covering the whole earth, yet, discrete gravity data is available only within a spherical cap in practice. A Combination of a global geopotential model (GGM, plural GGMs) with gravity data can

reduce the truncation error caused by this weakness. For optimal estimation of a gravimetric geoid, it is crucial to choose a GGM capable of recovering gravity field functionals (e.g., gravity anomalies, geoid undulations, and vertical deflections) that are comparable to those generated from GNSS-leveling and terrestrial gravity data.

To date, high-quality global gravity field models have been created from advanced satellite data or derived values with a spatial resolution of 9km, corresponding to a maximum degree of 2190[1]. The International Centre for Global Earth Models (ICGEM) is a service that provides the scientific community with a high-tech repository of static and temporal global gravity field models of the earth. About 180 GGMs are now available on the ICGEM's website (http://icgem.gfzpotsdam.de/ICGEM/-ICGEM.html).

Several studies have been conducted to determine the applicability of GGMs in Malaysia in general, and Peninsular Malaysia, in particular. In [2], a comparison was made between OSU91A and EGM96 GGMs. It was concluded that the EGM96 model could recover the short frequency signals of both the geoid undulations and the gravity anomalies better. In [3], the EIGEN-6C4 model was used to compute a gravimetric geoid model over Peninsular Malaysia because it provided the best fit amongst the combined models. In the same study, the GO_CONS_GCF _2_SPW_ R4 was considered best amongst the satellite only GGMs.

With the number of geopotential models growing every year, it will be difficult for the user to select the most optimum model for their regional modelling without testing each model. Moreover, different geopotential models perform differently in different wavelengths [4] and hence, the best overall geopotential model selected for an area may be weaker in some wavelengths, and vice-versa. Instead of using a single geopotential model, it would be desirable to get the best out of all available geopotential models.

This study aims to develop a combined geopotential model by extracting the best spectral information from a selection of the most recent and high-resolution GGMs from the International Center for Global Earth models (ICGEM) for future geoid modelling in Peninsular Malaysia. The models are first filtered using GNSS geoid undulations and observed gravity anomalies, to obtain the best performing model(s) from which to extract the spectral information. The new model's internal characteristics are tested together with other geopotential models using spectral analysis. Results show that combined geopotential models perform better than the individual geopotential models, and may improve the quality of regional geoid modelling.

2. Data used

The most recent and highest resolution GGMs, GNSS-levelled points, and point free-air anomalies were employed in this investigation. The following subsections provide an overview of the data set.

2.1. Global Geopotential models

A total of 30 GGMs were chosen for the study, all of which either have a maximum degree not less than 360 or were produced within the last ten years. The GGMs span a variety of models with various input information (e.g., terrestrial gravity, satellite tracking and altimetry data), as well as degree and order diversity. The present study includes models that had been examined and recommended in earlier Malaysian studies. In Table 1, the features of the GGMs, which were retrieved from the ICGEM website, are listed.

Table 1. Earth Gravity models (Refer to http://icgem.gfz-potsdam.de/tom_longtime).

S/N	Model	Degree	Year	Data[a]
1	SGG-UGM-2	2190	2020	A, Grace (GOCE), EGM2008
2	XGM2019e_2159	2190	2019	A, G, T, S(GOCO06s)
3	XGM2019e	5540	2019	A, G, T, S(GOCO06s)
4	XGM2019	760	2019	A, G, T, S(GOCO06s)
5	ITSG-Grace2018s	200	2019	S(Grace)

6	GOCO06s	300	2019	S
7	GO_CONS_GCF_2_TIM_R6	300	2019	S(Goce)
8	GO_CONS_GCF_2_DIR_R6	300	2019	S
9	IGGT_R1C	240	2018	G, S, S(Grace)
10	Tongji-Grace02k	180	2018	S(Grace)
11	SGG-UGM-1	2159	2018	EGM2008, S(Goce)
12	GOSG01S	220	2018	S(Goce)
13	IGGT_R1	240	2017	S(Goce)
14	IfE_GOCE05s	250	2017	S
15	GO_CONS_GCF_2_SPW_R5	330	2017	S(Goce)
16	XGM2016	719	2017	A, G, S(GOCO05s)
17	Tongji-Grace02s	180	2017	S(Grace)
18	EIGEN-6C4	2190	2014	A,G,S(Goce, Grace & Lageos)
19	GO_CONS_GCF_2_SPW_R4	280	2014	S(Goce)
20	GO_CONS_GCF_2_TIM_R4	250	2013	S(Goce)
21	EIGEN-6C	1420	2011	A,G,S(Goce,Grace & Lageos)
22	GO_CONS_GCF_2_TIM_R3	250	2011	S(Goce)
23	GO_CONS_GCF_2_DIR_R3	240	2011	S(Goce,Grace & Lageos)
24	GOCO02s	250	2011	S(Goce & Grace)
25	GOCO01s	224	2010	S(Champ & Grace)
26	EGM2008	2190	2008	A, G, S(Grace)
27	EIGEN-GL04C	360	2006	A, G, S(Grace & Lageos)
28	eigen-cg03c	360	2005	A, G, S(Champ & Grace)
29	EIGEN-CHAMP03S	140	2004	S(Champ)
30	EGM96	360	1996	A, EGM96S, G

[a] Data: G = Gravity data, S = Satellite tracking data, A = Altimetry data.

2.2. Gridded free air anomalies

A 30m by 30m resolution grid of surface free air anomalies was used. This grid was computed from terrestrial and air-borne data supplied by the Department of Survey and Mapping Malaysia (DSMM), and processed as explained in [5]. Table 2 shows the statistical indicators of the gravity data that was used in the investigation.

Table 2. Statistics of Gravity gridded data used.

	Min	Max	Mean	Std. Dev.
Free Air Anomalies	-103.405	337.528	18.229	26.996

2.3. GNSS-Levelling data

The selected geopotential models were validated using 173 GNSS-levelled sites acquired from the Department of Surveying and Mapping Malaysia (DSMM). Table 3 contains the height statistical indicators, whereas Figure 1 depicts the position of the data points.

Table 3. Statistics for height datasets for 173 GNSS-levelled points over Peninsular Malaysia (Units in metres).

	Min	Max	Mean	Std. Dev.
Ellipsoidal height, h:	0.965	334.339	34.313	42.001
Orthometric Height, H	-7.177	343.574	35.807	43.266
Observed undulations, $(h - H)$:	-14.330	10.294	-1.495	5.630

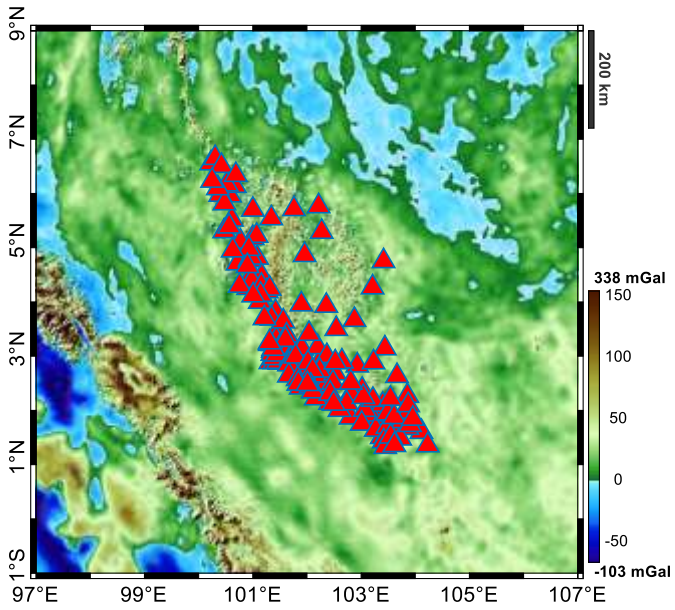

Figure 1. Map of free air anomalies used in the study. Red triangles indicate the positions of GNSS-levelled benchmarks.

3. Method

3.1. Synthesis of Gravity functionals

A Global geopotential model is a collection of dimensionless, fully normalized spherical harmonic coefficients $\bar{C}_{nm}$ and $\bar{S}_{nm}$ as well as their errors $\delta\bar{C}_{nm}$ and $\delta\bar{S}_{nm}$, that may be used to simulate the earth's gravity field. These coefficients were calculated using a combination of terrestrial and satellite gravity measurements or a study of satellite observations [6]. Geoid undulations, height anomalies, gravity anomalies, gravity disturbances, and vertical deflections, as well as other gravity field functionals implied by the related GGM, can all be calculated using the coefficients.

The disturbing potential, T is commonly represented by the expansion [7–10]: -

$$T(P) = \frac{GM}{r_p}\sum_{n=2}^{\infty}\left(\frac{a}{r_p}\right)^n \sum_{m=0}^{n}\left[\bar{C}_{nm}cos(m\lambda) + \bar{S}_{nm}sin(m\lambda)\right] P_{nm}cos(\varphi) \quad (1)$$

where GM is the earth's gravitational constant, a is the semi-major axis of the normal reference ellipsoid, r_P is the distance of a point P from the origin, $\bar{C}_{nm}$ and $\bar{S}_{nm}$ are the fully normalized spherical harmonic coefficients of the disturbing potential, P_{nm} are the fully normalized associated Legendre functions for degree n and order m, and (φ, λ) are spherical polar coordinates of point P. The coefficients $\bar{C}_{nm}$ $(n\ is\ even\ and\ m = 0)$ are referred to an ellipsoid of a given flattening.

Geoid undulations may be obtained by combining equation (1) with the Brun's equation to obtain [8–12]: -

$$N_{ggm} = N_0 + \frac{GM}{\gamma r}\sum_{n=2}^{n_{max}}\left(\frac{a}{r}\right)^n \sum_{m=0}^{n}\left[\bar{C}_{nm}Cosm\lambda + \bar{S}_{nm}Sin(m\lambda)\right] P_{nm}Sin(\varphi) \quad (2)$$

where GM is the product of the universal gravitational constant and the earth's mass, a is a scaling parameter related to a specific GGM, n_{max} is the geopotential model's maximum degree, and r, λ, φ are the geocentric coordinates of the geoid-reduced computation point.

Gravity anomalies may also be synthesized from the spherical harmonic coefficients using the equation [8–12]: -

$$\Delta g_{ggm} = \Delta g_0 + \frac{GM}{r^2}\sum_{n=2}^{nmax}\left(\frac{a}{r}\right)^n (n-1)\sum_{m=0}^{n}[\bar{C}_{nm}Cosm\lambda + \bar{S}_{nm}Sin(m\lambda)]\,P_{nm}Sin(\varphi) \quad (3)$$

where the quantities are as previously defined.

3.2. Zero-Degree Terms

With equations (2) and (3), the terms N_0 and Δg_0 are components of the zero-degree terms for the GGM geoid undulations and gravity anomalies, respectively, in relation to the reference normal ellipsoid. They allow the geoid undulation and gravity anomalies synthesized from GGMs to be linked to a specific equipotential surface with W_0 and GM_E values, by accounting for the changes in masses and potential between the geopotential model utilized and the reference ellipsoid. They may be computed from the formulae [9,13,14]: -

$$N_0 = \frac{GM - GM_E}{R\gamma} - \frac{W_0 - U_0}{\gamma} \quad (4)$$

$$\Delta g_0 == \frac{GM_E - GM_0}{r^2} - \frac{2(W_0 - U_{0)}}{r} \quad (5)$$

where the normal ellipsoid is represented by the parameters GM_E and U_0 [15] to create the Somigliana-Pizzeti normal gravity field.

3.3. Selection of Permanent Tide

Global Geopotential models are provided either in the zero-tide or tide-free, or in both versions [16]. The mean-tide potential cannot be employed in gravity field modelling because it comprises the permanent tide-generating potential, which is generated by masses exterior to the Earth. For an explanation of the pros and cons of using the different permanent tides, the reader is referred to e.g. [16–18]. Concerning spherical harmonic coefficients, only the C_{20} coefficient is affected by the permanent tide. Depending on the desired permanent tide to be used, the C_{20} coefficients of the selected GGMs may be transformed into the new system using the relation [19,20]: -

$$C^{T-F}{}_{20} = C^{Z-T}{}_{20} + 3.1108 \times 10^{-8} \times \frac{k_2}{\sqrt{5}} \quad (6)$$

where $C^{T-F}{}_{20}$ and $C^{Z-T}{}_{20}$ are the spherical harmonic coefficients in the tide-free and zero-tide systems, respectively, and $k_2 = 0.3$ is the adopted second-degree love number.

In Peninsular Malaysia, surveying and mapping activities are referred to the Peninsular Geodetic Vertical Datum (PMGVD), which is based on 10 years of tidal observation data[21,22]. The datum was transferred from 0 at the Port Kelang tide gauge to 3.624m at a memorial monument using a combination of precise levelling and gravity survey. Due to lack of luni-solar correction to precise leveling in Peninsular Malaysia, orthometric heights are automatically reported in the mean tide system [18]. In order to have all quantities in the same permanent tide, these heights may be converted into the tide free system and vice-versa using the formulae [22,23]: -

$$H^{T-F} = H^{M-T} + 0.680(0.099 - 0.296sin^2\varphi) \quad (7)$$

where H^{T-F} and $H^{M-T}$are the tide-free and mean-tide levelling heights, respectively and φ is the geodetic latitude of the GNSS-levelled benchmark.

3.4. Spectral analysis of GGMs

3.4.1. Degree variances and error degree variances. Using spherical harmonic coefficients, the signal degree variances of the anomalous potential may be calculated from [24,25]: -

$$c_n = k^2 \sum_{m=0}^{n} (\bar{C}_{nm}{}^2 + \bar{S}_{nm}{}^2) \tag{8}$$

and the error degree variances by[24,25]:-

$$\delta c_n = k^2 \sum_{m=0}^{n} (\delta\bar{C}_{nm}{}^2 + \delta\bar{S}_{nm}{}^2) \tag{9}$$

where quantities are as defined previously.

Equations (8) and (9) are applicable to all functionals of the gravity field provided the appropriate eigenvalue, k is inserted in the equations. The factor k corresponding to the various functionals of the disturbing potential are given in Table 4.

Table 4. Signal factors of some gravity functionals [24].

Gravity functional	Symbol	Factor, k	unit
Signal	c	1	unit-less
Disturbing potential	T	$\frac{GM}{R}$	$m^2 s^{-2}$
Geoid height	N	R	m
Gravity anomaly	Δg	$\frac{GM}{R^2}(n-1)\times 10^5$	mGal
Gravity disturbance	δg	$\frac{GM}{R^2}(n+1)\times 10^5$	mGal
Vertical deflection	θ	$180 \times \frac{3600}{\pi}$	degree-sec
Vertical gravity gradient	δg_r	$\frac{GM}{R^3}(n+1)(n+2)\times 10^8$	mGal km^{-1}

The signal degree variance signifies the amount of signal power implied by all the coefficients within a specific degree and is commonly referred to as the power spectrum. Conversely, the error degree variance is an expression of how much signal power error of a given anomalous quantity exists for all the coefficients of a specific degree. The variation of power spectra with the degree may therefore be used to describe the rate of decay of the anomalous signal as the degree increases.

3.4.2. Root mean square error. The root mean square (RMS) by degree of gravity functionals may be computed from [4,24,25]: -

$$c^{rms}{}_n = k\sqrt{\frac{\sum_{m=0}^{n}(\bar{C}_{nm}{}^2 + \bar{S}_{nm}{}^2)}{n^2}} \tag{10}$$

while the overall RMS may be obtained from [24,25]: -

$$\sigma_T = \left(\sum_{n=2}^{\infty} {c^{rms}}_n \right)^{\frac{1}{2}} \tag{11}$$

In this study, the root mean squares of the geoidal undulations and gravity anomalies were estimated by the wavelength of the selected geopotential models. Four wavelength types were selected as defined in [4]: -

1. Long wavelengths: gravity field information ranging from degrees n=2 to n=10, equivalent to a linear half-wavelength of 2000km and greater.
2. Intermediate wavelength: for gravity field information ranging from degrees n=11 to n=100 equivalent to a linear half-wavelength of 200 to 2000km.
3. Short wavelength: gravity field information ranging from degrees n=101 to n=1000 equivalent to a linear half-wavelength of 20 to 200km.
4. Very short wavelength: gravity field information ranging from degrees 1001 to ∞ equivalent to a linear half-wavelength less than 20km.

The total RMS of the point gravity field functional may be expressed in terms of its wavelength components from [4]: -

$$\sigma_T = \left[{\sigma_{2,10}}^2 + {\sigma_{11,100}}^2 + {\sigma_{101,1000}}^2 + {\sigma_{>1000}}^2 \right]^{\frac{1}{2}} \tag{12}$$

3.4.3. Signal to Noise ratio. The signal-to-noise (SNR) ratio may be computed both cumulatively or by degree. The SNR by degree may be obtained from [26]: -

$$S_{nr} = \frac{c_n}{\delta c_n} \tag{13}$$

where variables are as previously defined.

3.5. Comparison with GNSS-levelled heights

3.5.1. Computation of bias. Observed Geoid heights, N_{gnss} may be computed from spirit-levelled orthometric heights, H and GNSS-measured ellipsoidal heights, h using the famous equation [27]: -

$$N_{gnss} = h - H \tag{14}$$

These heights are independent of the gravimetrically derived geoid heights, making them appropriate for evaluating geoid models, including GGMs. Equation (2) was used to determine the model-derived geoid undulations implied by the GGMs. The differences or bias for each GGM was computed for statistical analysis using the following equation [27]: -

$$\delta N = N_{gnss} - N_{ggm} \tag{15}$$

where N_{ggm} is the geoid height obtained from the GGM.

The basic statistical indicators, such as the mean, minimum, maximum and standard deviation, were then obtained.

3.5.2. Detection of outliers. To assess the quality of the GNSS-levelled points, the observed geoid undulations may be compared with undulations implied by a high resolution GGM as in equation (15). Standardized residuals are then computed using: -

$$v_{std} = \frac{v_i}{\sigma} \tag{16}$$

where v_i is the point residual and σ is the standard deviation.

Observations with a standard residual >3 were considered as outliers in this study.

3.5.3. Fitting of parametric models. To minimize the effect of systematic errors and datum inconsistencies [28,29] between the GNSS-levelling derived geoid undulations and those derived from GGMs, various parametric models were fitted into the observations using the equation [27]:-

$$\delta N = Ax \tag{17}$$

where x denotes a vector of the unknown parameters, and A is a design matrix corresponding to the unknown coefficients of a pre-selected parametric model. In this study, three, four, five and seven parametric models were used, respectively as follow[30]: -

Three parameters:

$$A = [cos\varphi cos\lambda \quad cos\varphi sin\lambda \quad sin\varphi] \tag{18}$$

Four parameters:

$$A = [1 \quad cos\varphi cos\lambda \quad cos\varphi sin\lambda \quad sin\varphi] \tag{19}$$

Five parameters:

$$A = [1 \quad cos\varphi cos\lambda \quad cos\varphi sin\lambda \quad sin\varphi \quad sin^2\varphi] \tag{20}$$

Seven parameters:

$$A = \left[cos\varphi cos\lambda \quad cos\varphi sin\lambda \quad sin\varphi \quad \frac{cos\varphi sin\varphi sin\lambda}{w} \quad \frac{cos\varphi sin\varphi cos\lambda}{w} \quad \frac{1 - f^2 sin^2\varphi}{w} \quad \frac{sin^2\varphi}{w}\right] \tag{21}$$

where f and e are the flattening and first eccentricity, respectively of the reference ellipsoid and w is given by $\sqrt{1 - e2sin2\varphi}$.

The unweighted least-squares adjustment was used since there was no information on the accuracy of both the observed and the synthesized geoid undulations. The solution to the least-squares adjustment was of the form [31,32]: -

$$X = (A^T PA)^{-1}(A^T L) \tag{22}$$

$$v = AX - L \tag{23}$$

$$\sigma = \sqrt{\frac{v^T V}{r}} \tag{24}$$

where v is the vector of residuals, σ the standard deviation, $r = n - m$, the degrees of freedom, n the number of evaluation points and m the number of parameters in terms of the parametric model.

3.5.4. Comparison with gravity anomalies. To carry out the assessment using gravity anomalies, 1000 points were randomly selected within the study area, and free-air gravity anomalies interpolated at their positions, using the MATLAB in-built function *interp2*. At the same points, gravity anomalies were obtained from synthesis of the selected GGMs using equation (3), with the resulting residual anomalies computed without terrain effects using the equation [33]: -

$$\Delta g = \Delta g_{fa} - \Delta g_{ggm} \tag{25}$$

3.6. Combined GGM

The combined GGM was obtained by comparing the signal to noise ratio of the geoid undulation and gravity anomaly spectra by degree, for all the selected GGMs. The coefficients $\bar{C}_{nm}$ and $\bar{S}_{nm}$, (and their errors), whose GGM provided the largest signal to noise ratio for a particular degree were selected for the combined GGM. The mass and the radius of the combined model was calculated from a weighted mean of the values given for the selected GGMs.

4. Results and Discussion

External validation was performed on all 30 GGMs utilizing 173 GNSS-leveled locations and observed free-air anomalies. On the GNSS-leveled points, an outlier detection mechanism was used by comparing the observed geoid undulations with those obtained from EGM2008, one of the highest resolution GGMs. Using the approaches of section 3.5.2, one outlier was identified and removed.

4.1. Computation of observed gravity field functionals

From the known orthometric and ellipsoidal heights of the GNSS-levelled stations, observed geoid heights were estimated using equation (14). 1000 plots were then randomly selected within the study area and free air anomalies were interpolated from the free air anomaly grid. The statistics of the observed GNSS undulations and interpolated free air anomalies are shown in Table 5.

Table 5. Statistical indicators for observed geoid undulations and free-air anomalies used at 1000 points (Units in metres for undulations and mGal for gravity anomalies).

	Min	Max	Mean	Std Dev.
Observed undulations(h-H)	-29.643	-12.700	-20.137	6.231
Observed Free air Anomalies	-22.344	20.147	-4.363	11.424

4.2. Synthesis of gravity field functionals

Equations (2) and (3) were used to synthesize geoid undulations and free air anomalies from the geopotential models at the GNSS-levelled points and at the 1000 random points, respectively, using MATLAB functions developed by the authors. The earth's geocentric gravitational constant (GM_E), and other constants, were derived from the GGMs.

4.3. Computation of Zero-Degree Terms

The zero-degree terms for the geoid undulation and free air anomalies were first computed for each GGM using equations (4) and (5), and the results were added to the synthesized gravity field functionals. A value of GM_E =3.986004415e14 was used in all GGMs. The reference ellipsoid provided the reference gravitational constant, GM_0, the mean Earth radius, R, the normal potential, U_0, and the mean normal gravity, γ. For the WGS84 ellipsoid [34], $GM_0 = 3.986004.418\text{e}14$, $U_0 = 62636851.7146$, $R = 6371008.771$, and $\gamma = 9.797643222$ m s^{-2}. The constant gravity potential of

the geoid was set as W_0=62636853.4 m2s-2, which was adopted as a realization of the potential value for the International Height Reference System (IHRS) during the 2015 International Union of Geodesy and Geophysics (IUGG) General Assembly [20,35]. For the WGS84 ellipsoid, mean values of -0.1768 m and -0.052 mGal of zero-degree terms were obtained for the geoid undulation and free air anomalies, respectively, for all the GGMs.

4.4. Comparison using GNSS-levelled points

The differences between the geometric and the GGM-based geoid undulations were computed using equation (15), and Table 6 shows the statistical indicators of the results. In the table, the GGMs are ranked in ascending order of the standard deviations obtained.

Table 6. Statistical Results of the differences between the GNSS-based and the GGM-based geoid undulations (units are in metres).

Model	Max Degree	Min	Max	Mean	Std Dev.
XGM2019e_2159	2190	0.110	0.601	0.317	0.071
XGM2019e	5540	0.118	0.609	0.319	0.071
EIGEN-6C	1420	0.049	0.607	0.334	0.083
SGG-UGM-1	2159	0.073	0.630	0.349	0.083
SGG-UGM-2	2190	0.027	0.590	0.324	0.086
EGM2008	2190	0.094	0.701	0.334	0.090
EIGEN-6C4	2190	0.144	0.684	0.366	0.091
XGM2019	760	-0.033	0.602	0.302	0.096
XGM2016	719	-0.028	0.595	0.300	0.096
GO_CONS_GCF_2_TIM_R6	300	-0.231	0.563	0.271	0.134
GOCO06s	300	-0.239	0.573	0.275	0.135
GO_CONS_GCF_2_DIR_R6	300	-0.229	0.577	0.304	0.137
GOCO01s	224	-0.093	0.669	0.315	0.144
GO_CONS_GCF_2_SPW_R5	330	-0.138	0.565	0.303	0.150
GO_CONS_GCF_2_SPW_R4	280	-0.048	0.642	0.316	0.154
GOCO02s	250	-0.129	0.712	0.309	0.162
IfE_GOCE05s	250	-0.146	0.726	0.304	0.164
GO_CONS_GCF_2_TIM_R4	250	-0.140	0.683	0.303	0.169
GO_CONS_GCF_2_DIR_R3	240	-0.066	0.733	0.324	0.170
GOSG01S	220	-0.272	0.632	0.279	0.179
IGGT_R1C	240	-0.195	0.795	0.211	0.187
GO_CONS_GCF_2_TIM_R3	250	-0.176	0.749	0.327	0.188
IGGT_R1	240	-0.223	0.826	0.224	0.228
EIGEN-GL04C	360	-0.242	0.876	0.317	0.232
ITSG-Grace2018s	200	-0.316	0.781	0.182	0.259
eigen-cg03c	360	-0.365	0.854	0.268	0.263
Tongji-Grace02s	180	-0.337	0.914	0.190	0.314
Tongji-Grace02k	180	-0.364	0.901	0.188	0.315
EGM96	360	-0.573	0.763	0.051	0.333
EIGEN-CHAMP03S	140	-0.315	1.710	0.445	0.532

As shown by the mean values in Table 6, there is evidence of some bias between the geopotential of the Malaysian vertical datum's zero-height surface and the equipotential surface specified by the IERS conventional value Wo = 62636856.00 m2/s2, which was used in the development of most of the selected GGMs. Long and medium wavelength inaccuracies in the spherical harmonic coefficients are most likely to blame for these discrepancies [36,37].

Least-squares parametric fitting was used to model the systematic errors using the models mentioned in section 3.5. The residuals were then combined with the observations (h-H), and the results were compared to the GNSS-level undulations. As indicated in Table 9, this improved the standard deviations.

Table 7. Standard deviations of the differences of geoid undulations $N_{gnss} - N_{ggm}$, after the least-squares fit with selected models at the 172 GNSS/levelling benchmarks (units are in metres).

Model	Max Degree	Parametric Model (No. of parameters)			
		3	4	5	7
SGG-UGM-2	2190	0.08187	0.07816	0.07750	0.06438
XGM2019e_2159	2190	0.07103	0.06878	0.06847	0.06147
XGM2019e	5540	0.07102	0.06902	0.06853	0.06142
XGM2019	760	0.09510	0.09493	0.09490	0.08226
ITSG-Grace2018s	200	0.24251	0.24165	0.22168	0.21376
GOCO06s	300	0.13036	0.12675	0.12647	0.10381
GO_CONS_GCF_2_TIM_R6	300	0.12915	0.12544	0.12510	0.10194
GO_CONS_GCF_2_DIR_R6	300	0.13252	0.12888	0.12879	0.10144
GO_CONS_GCF_2_SPW_R4	280	0.13538	0.13438	0.13424	0.10224
IGGT_R1C	240	0.17746	0.17636	0.15988	0.14766
Tongji-Grace02k	180	0.26897	0.23205	0.22243	0.20383
SGG-UGM-1	2159	0.08053	0.07743	0.07629	0.06169
GOSG01S	220	0.15603	0.15503	0.15472	0.11833
IGGT_R1	240	0.22549	0.21283	0.21233	0.20725
IfE_GOCE05s	250	0.15475	0.14854	0.13632	0.11489
GO_CONS_GCF_2_SPW_R5	330	0.13901	0.13449	0.13426	0.12092
XGM2016	719	0.09530	0.09508	0.09502	0.08241
Tongji-Grace02s	180	0.26624	0.22942	0.21832	0.20073
EIGEN-6C4	2190	0.08838	0.08643	0.08600	0.06850
EIGEN-6C	1420	0.08224	0.08208	0.08170	0.06748
GO_CONS_GCF_2_TIM_R4	250	0.15083	0.14162	0.13601	0.11737
GO_CONS_GCF_2_TIM_R3	250	0.16523	0.15425	0.15241	0.14571
GO_CONS_GCF_2_DIR_R3	240	0.14845	0.14163	0.14137	0.13046
GOCO02s	250	0.14951	0.13620	0.13617	0.13399
GOCO01s	224	0.13388	0.12777	0.12773	0.12586
EGM2008	2190	0.08766	0.08751	0.08747	0.06926
EIGEN-GL04C	360	0.22877	0.22390	0.21863	0.20953
eigen-cg03c	360	0.25395	0.24640	0.23914	0.22747
EIGEN-CHAMP03S	140	0.33844	0.22910	0.20282	0.16602
EGM96	360	0.19580	0.19008	0.18837	0.16259

Among the selected GGMs, the XGM_2019_2159 and XGM_2019e produced the lowest standard deviation of 0.071m each of the difference between GNSS based and geopotential-based undulations. Generally, most of the higher resolution GGMs (>360) performed well with standard deviations < 0.1m. Among the Satellite only GGMs, GO_CONS_GCF_2_TIM_R6, GOCO06s and GO_CONS_GCF_2_DIR_R6 performed best with standard deviations of 0.134. 0.135 and 0.137m respectively. After removal of the systematic errors, the standard deviation improved in all models, with the higher resolution GGMs still performing better than lower resolution GGMs. When the parametric models were compared, the seven-parametric model produced lower standard deviations for all GGMs, hence it was used to rank the GGMs' performance in terms of undulations.

. Overall, the XGM_2019e, XGM_2019e_2159 and SGG-UGGM1 produced the best fit with standard deviations of 0.0615, 0.0615 and 0.0617 m, respectively, with all the high resolution GGMs obtaining < 9cm standard deviations. For the satellite only GGMs, GO_CONS_GCF_2_DIR_R6,

GO_CONS_GCF_2_TIM_R6 and GO_CONS_GCF_2_SPW_R4 were the best performers with standard deviations of 0.1014, 0.1019 and 0.1022 m respectively.

4.5. Comparison using free air anomalies

The free-air gravity anomalies synthesized using the geopotential models were compared to the observed free-air anomalies at the 1000 random points. The residual anomalies were produced after subtracting the synthetic anomalies from the observed anomalies, and the statistical results are reported in Table 8.

Table 8. Statistics of residual free air anomalies over Peninsular Malaysia referred to the selected GGMs at 1000 random points (Units are in mGal).

Model	Max Degree	Min	Max	Mean	Std Dev.
EGM2008	2190	-61.282	42.926	-0.024	8.149
SGG-UGM-1	2159	-59.987	43.473	-0.033	8.187
EIGEN-6C	1420	-61.963	56.605	-0.306	8.349
SGG-UGM-2	2190	-58.919	43.919	0.013	8.393
EIGEN-6C4	2190	-60.593	43.905	0.053	8.628
XGM2019e_2159	2190	-58.276	65.293	-0.028	8.753
XGM2019e	5540	-70.011	64.868	0.317	8.855
XGM2019	760	-70.205	82.276	-0.433	10.363
XGM2016	719	-69.750	82.149	-0.477	10.386
GO_CONS_GCF_2_SPW_R5	330	-80.647	90.795	-0.471	14.407
EGM96	360	-70.367	111.843	-0.571	14.432
GO_CONS_GCF_2_DIR_R6	300	-77.780	96.030	-0.665	14.433
GO_CONS_GCF_2_TIM_R6	300	-77.213	95.115	-0.679	14.468
GOCO06s	300	-77.240	95.723	-0.677	14.483
eigen-cg03c	360	-73.473	113.277	0.042	14.500
EIGEN-GL04C	360	-69.965	113.126	-0.079	14.570
IfE_GOCE05s	250	-75.611	94.294	-0.703	14.723
GO_CONS_GCF_2_SPW_R4	280	-74.645	95.738	-0.454	14.833
IGGT_R1	240	-73.894	93.918	-0.548	14.945
GOCO01s	224	-77.281	98.853	-0.677	15.143
GO_CONS_GCF_2_TIM_R4	250	-77.575	91.994	-0.608	15.174
IGGT_R1C	240	-74.583	99.309	-0.768	15.298
GO_CONS_GCF_2_DIR_R3	240	-81.975	90.284	-0.493	15.305
GO_CONS_GCF_2_TIM_R3	250	-82.576	90.266	-0.506	15.443
GOCO02s	250	-80.262	91.265	-0.548	15.469
GOSG01S	220	-75.698	95.119	-0.676	15.510
Tongji-Grace02k	180	-70.379	115.317	-0.595	16.871
ITSG-Grace2018s	200	-77.948	100.734	-0.700	16.872
Tongji-Grace02s	180	-70.606	116.142	-0.589	16.944
EIGEN-CHAMP03S	140	-54.978	143.038	-0.546	19.010

As can be observed from Table 8, the higher resolution GGMs outperformed the lower ones. EGM2008, SGG-UGM-1 and EIGEN-6C produced the best fit in terms of gravity anomalies in Peninsular Malaysia because of their low standard deviations of 8.149, 8.187 and 8.349 mGal, respectively.

4.6. Computation of combined GGM

From the previous evaluation, ten of the best ranked GGMs in each category were selected for the purpose of comparing their spectral behavior, in terms of the signal to noise ratio of the disturbing potential. The selected GGMs are depicted in Table 9.

Table 9. Selected GGMs for the combined model.

Model	Max Degree	Permanent Tide	Data
EGM2008	2190	Tide-free	A, G, S(Grace)
SGG-UGM-1	2159	Tide-free	EGM2008, S(Goce)
EIGEN-6C	1420	Tide-free	A,G,S(Goce, Grace & Lageos)
SGG-UGM-2	2190	Zero-tide	A, EGM2008, Grace(GOCE)
EIGEN-6C4	2190	Tide-free	A,G,S(Goce, Grace & Lageos)
XGM2019e_2159	2190	Zero-tide	A, G, T, S(GOCO06s)
XGM2019e	5540	Zero-tide	A, G, T, S(GOCO06s)
XGM2019	760	Zero-tide	A, G, T, S(GOCO06s)
XGM2016	719	Zero-tide	A, G, T, S(GOCO05s)
GO_CONS_GCF_2_SPW_R5	330	Tide-free	S(Goce)
EGM96	360	Tide-free	A, EGM96S, G
GO_CONS_GCF_2_DIR_R6	300	Tide-free	S
GO_CONS_GCF_2_TIM_R6	300	Zero-tide	S(Goce)
GOCO06s	300	Zero-tide	S
EIGEN-GL04C	360	Tide-free	A, G, S(Grace & Lageos)
IGGT_R1	240	Tide-free	S(Goce)

4.6.1. Selection of permanent tide. The tide-free system was used in computation of the new geopotential model, since this is the system used for the ITRF coordinate system to evaluate geopotential models. All geopotential models were therefore converted into the tide-free system by changing the C_{20} coefficient as in equation (6). The results of the conversion for the selected models are depicted in Table 10.

Table 10. Transformation of selected GGMs to Tide-free Permanent Tide system.

Model	Permanent Tide	C_{20}	C_{20} (Tide Free)
EGM2008	tide-free	-4.841651437908e-04	-4.841651437908e-04
SGG-UGM-1	tide-free	-4.841653985950e-04	-4.841653985950e-04
EIGEN-6C	tide-free	-4.841652998060e-04	-4.841652998060e-04
SGG-UGM-2	zero-tide	-4.841687322752e-04	-4.841645586990e-04
EIGEN-6C4	tide-free	-4.841652170610e-04	-4.841652170610e-04
XGM2019e_2159	zero-tide	-4.841694947476e-04	-4.841653211714e-04
XGM2019e	zero-tide	-4.841694947476e-04	-4.841653211714e-04
XGM2019	zero-tide	-4.841694947476e-04	-4.841653211714e-04
XGM2016	zero-tide	-4.841694588725e-04	-4.841652852963e-04
GO_CONS_GCF_2_SPW_R5	tide-free	-4.841651931193e-04	-4.841651931193e-04
EGM96	tide-free	-4.841653717360e-04	-4.841653717360e-04
GO_CONS_GCF_2_DIR_R6	tide-free	-4.841653013850e-04	-4.841653013850e-04
GO_CONS_GCF_2_TIM_R6	zero-tide	-4.841698526336e-04	-4.841656790574e-04
GOCO06s	zero-tide	-4.841694947139e-04	-4.841653211377e-04
EIGEN-GL04C	tide-free	-4.841652270940e-04	-4.841652270940e-04
IGGT_R1	tide-free	-4.841653618140e-04	-4.841653618140e-04

4.6.2. Optimization of harmonic coefficients. Using the spherical harmonic coefficients, the signal to noise ratio of the disturbing potential was computed per degree for all GGMs selected. The disturbing potential was used since all other gravity field functionals are its derivatives, and therefore related to them. For every degree, up to a maximum of 2500, the coefficients and their error estimates producing the larger signal to noise ratio were selected for the combined GGM. The mass of the earth and reference radius were adopted from a weighted mean of the values used for the selected GGMs. Values of 3.9860044150e14 and 6378136.3874 were obtained for the earth's gravitational constant and its radius, respectively. Table 11 shows the GGMs whose coefficients were selected for the respective degree and order.

Table 11. Harmonic coefficients used for combined model.

Degree	Model
3,5,7	Eigen-6C
4,6,8-25	XGM2016
26-134	SGG-UGM-2
135-341	XGM2016
342-371	Eigen-6C
372-2166	Eigen-6C4
2167-2190	XGM2019e_2159
2191-2500	XGM2019e

From the results of Table 11, the combined model was derived from 6 GGMs, with Eigen-6C containing most of the very short wavelength coefficients, according to the classification of section 3.4. In Table 12, a sample of the normalized spherical harmonic coefficients of the model, which was called PM_com_1c in this study, is shown. Figure 2 and Figure 3 depict the geoid undulations and free air anomalies, respectively, implied by the new model.

Table 12. Sampled normalized spherical harmonic coefficients of the earth gravity potential derived from PM_com_1c model.

Degree	Order	C_{nm}	S_{nm}	ΔC_{nm}	ΔS_{nm}
0	0	1.000000000000e+00	0.000000000000e+00	0.0000e+00	0.0000e+00
1	0	0.000000000000e+00	0.000000000000e+00	0.0000e+00	0.0000e+00
1	1	0.000000000000e+00	0.000000000000e+00	0.0000e+00	0.0000e+00
2	0	-4.841652998060e-04	0.000000000000e+00	1.9482e-13	0.0000e+00
2	1	-2.816400423460e-10	1.442559001660e-09	1.6940e-13	1.6997e-13
2	2	2.439358180070e-06	-1.400285283900e-06	1.8060e-13	1.7953e-13
10	0	5.334292240168e-08	0.000000000000e+00	4.7795e-14	0.0000e+00
10	1	8.375393702468e-08	-1.310940104858e-07	4.3591e-14	4.4183e-14
140	0	3.684813882117e-10	0.000000000000e+00	1.9272e-12	0.0000e+00
140	1	8.735761895555e-10	6.647449286330e-10	1.9050e-12	1.9493e-12
1000	0	-6.798854692000e-12	0.000000000000e+00	1.7420e-13	0.0000e+00
1000	1	-3.281591849200e-12	7.899423709300e-13	1.7400e-13	1.7400e-13
2189	2189	0.000000000000e+00	0.000000000000e+00	0.0000e+00	0.0000e+00
2190	0	-4.151773276016e-13	0.000000000000e+00	2.2758e-13	0.0000e+00
2500	2499	-5.999881589916e-13	4.856041138398e-13	4.9074e-13	4.9074e-13
2500	2500	2.706411725827e-13	-1.448432016773e-13	4.9239e-13	4.9239e-13

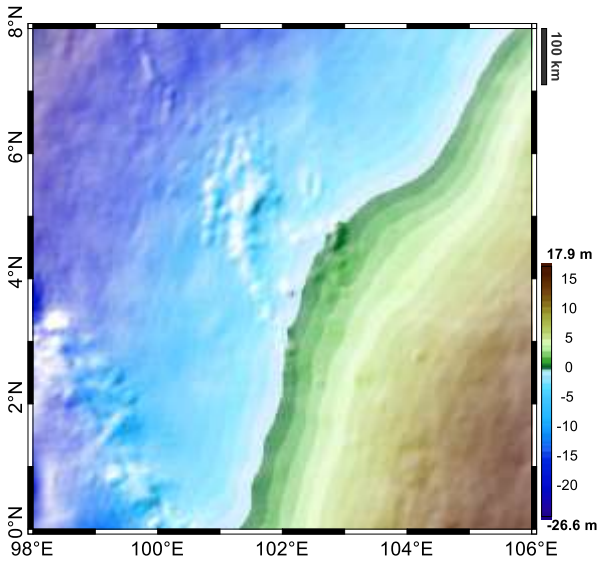

Figure 2. Geoid undulations for the new combined geopotential model, PM_com_1c.

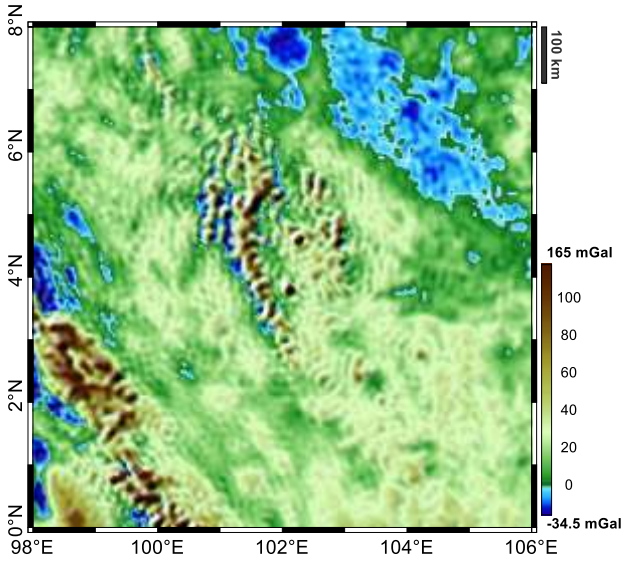

Figure 3. Free air anomalies for the new combined geopotential Model, PM_com_1c.

4.7. Validation of New Geopotential model

The new geopotential model was validated by comparing its spectral information with the other GGMs used in this study. Using the procedures of section *3.4*, the signal and error spectra of different gravity functionals were compared up to a maximum degree of *2*500.

4.7.1. Comparison of GGMs using SNR. Table 13 shows the results of the SNR of the signal and error spectra by wavelength, respectively, in terms of both gravity anomaly and geoid undulation.

Table 13. Geoid undulation and Gravity anomaly S2N ratio by wavelength.

Model	Max Degree	Long 3<N<=10	Intermediate 10<N<=100	Short 100<N<=1000	Very Short N>1000	Total
EGM2008	2190	629.733	372.568	74.740	40.378	736.605
SGG-UGM-1	2159	804.119	520.671	151.881	38.833	970.712
EIGEN-6C	1420	3495.075	2120.119	179.733	74.040	4092.462
SGG-UGM-2	2190	2099.257	2197.064	218.095	51.302	3046.994
EIGEN-6C4	2190	2790.123	1838.613	217.701	121.674	3350.743
XGM2019e_2159	2190	2028.673	2036.025	191.793	54.239	2881.083
XGM2019e	2500	2028.673	2036.025	191.793	59.842	2881.194
XGM2019	760	2029.367	2032.011	190.423	-	2878.135
XGM2016	719	3358.519	2410.699	211.758	-	4139.561
GO_CONS_GCF_2_SPW_R5	330	299.293	164.781	51.513	-	345.518
EGM96	360	97.828	38.593	23.408	-	107.739
GO_CONS_GCF_2_DIR_R6	300	2032.053	1280.060	151.496	-	2406.396
GO_CONS_GCF_2_TIM_R6	300	668.928	485.109	103.652	-	832.790
GOCO06s	300	2031.747	2036.949	162.430	-	2881.587
EIGEN-GL04C	360	539.030	477.493	32.856	-	720.855
PM_com_1c	2500	3595.511	2522.494	278.005	124.620	4402.669
IGGT_R1	240	207.115	287.884	63.429	-	360.274

From the analysis of Table 13, the new combined geopotential model produced the largest signal to noise ratio in the disturbing potential, gravity anomaly and geoid undulation which, expectedly, had the same values across the whole spectrum under investigation. The same can be said of Figure 4 and Figure 5 where the signal to noise ratios are plotted by harmonic degree for the gravity anomaly and geoid undulation, respectively.

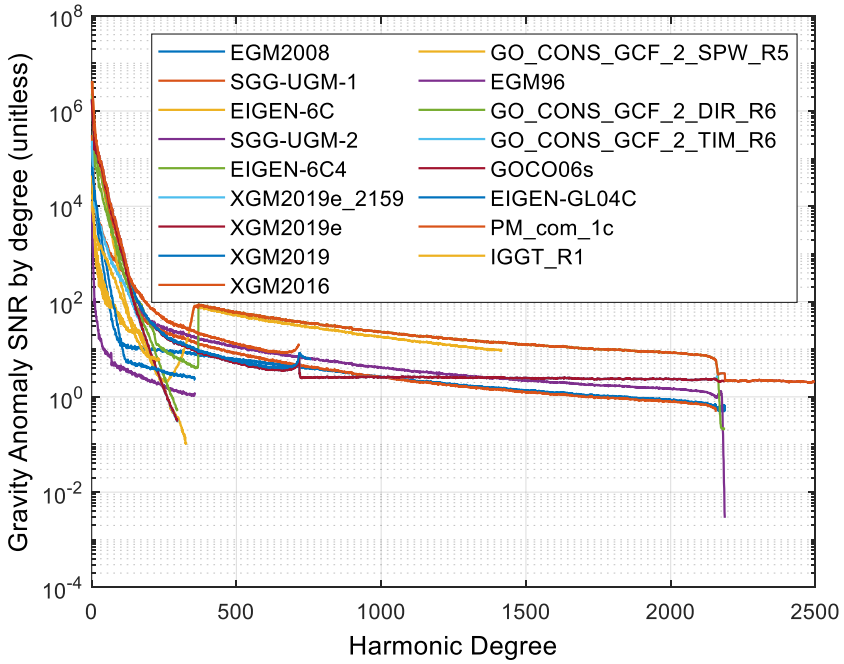

Figure 4. Gravity anomaly signal to noise ratio.

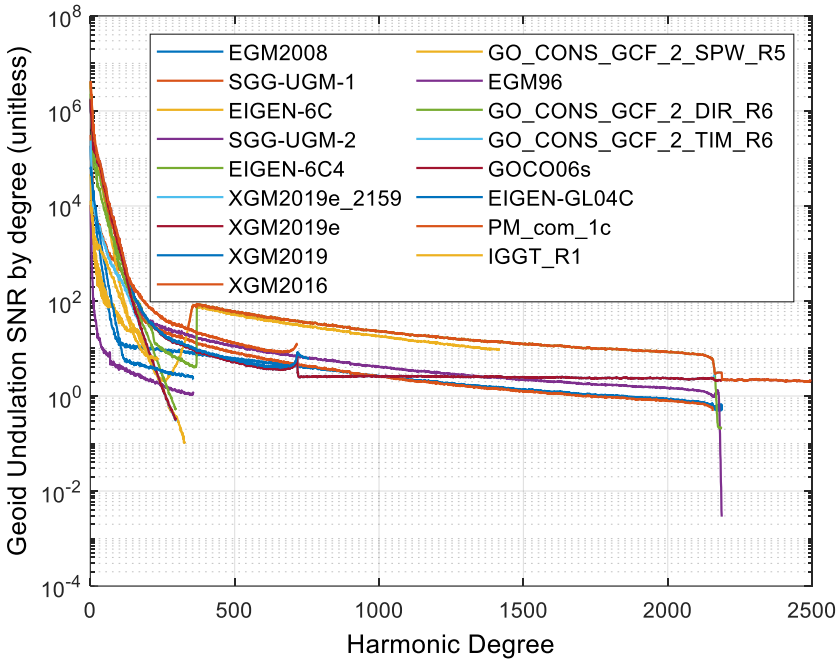

Figure 5. Geoid undulation signal to noise ratio.

4.7.2. Comparison of GGMs using error spectra. The cumulative errors of the gravity anomaly and geoid undulation signal are depicted in Figure 6 and Figure 7, respectively, by harmonic degree according to equation (12).

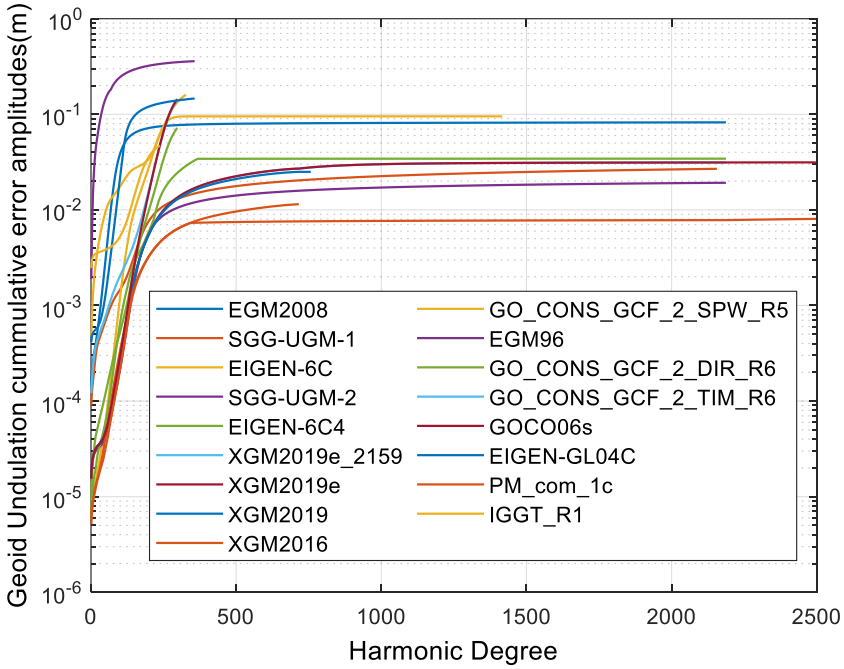

Figure 6. Geoid undulation cumulative error amplitudes.

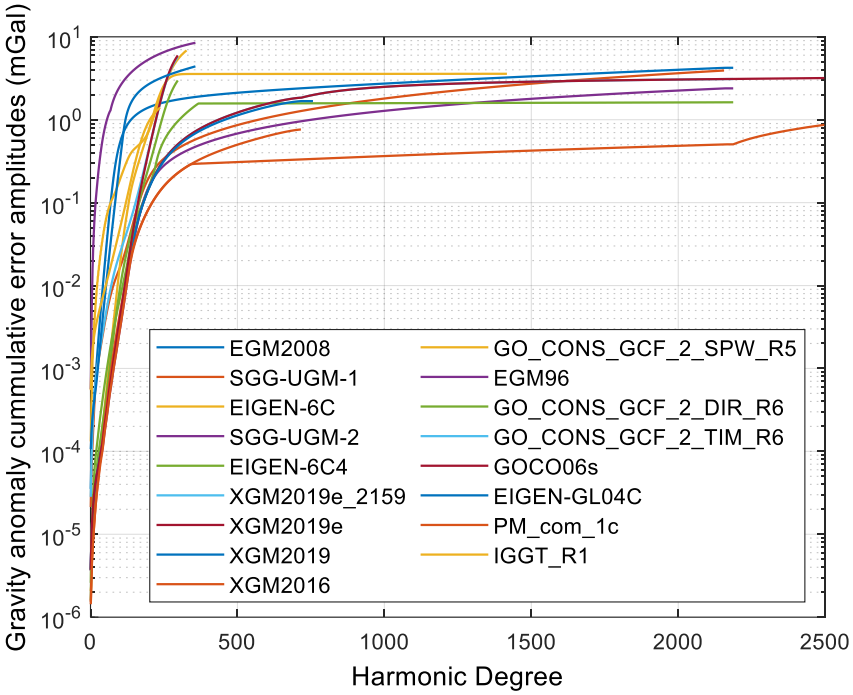

Figure 7. Gravity anomaly cumulative error amplitudes.

From the above figures, the new GGM exhibits a lower cumulative error spectra in terms of both the gravity anomalies and geoid undulations.

5. Conclusion

This study developed a combined geopotential model from a selection of the best performing, most recent and highest resolution GGMs available at the ICGEM. The models were selected based on their fit to a set of collocated GNSS-spirit levelled points and a grid of gravity anomalies covering the Peninsular Malaysia.

From the geometrical comparison of selected GGMs, it was revealed that the XGM_2019_2159 and XGM_2019e produced the lowest standard deviation of 0.071m each of the difference between GNSS based and geopotential-based undulations. Most of the higher resolution GGMs (>360), however, performed well with standard deviations < 0.1m. Among the Satellite only GGMs, GO_CONS_GCF_2_TIM_R6, GOCO06s and GO_CONS_GCF_2_DIR_R6 performed best with standard errors of 0.134. 0.135 and 0.137m respectively. After removal of the systematic errors, the standard deviation improved in all models, with the higher resolution GGMs still performing better than lower resolution GGMs. Overall, the XGM_2019e, XGM_2019e_2159 and SGG_UGM_1 produced the best fit with standard errors of 0.0614, 0.0615 and 0.0619m, respectively. For the satellite only GGMs, GO_CONS_GCF_2_DIR_R6, GO_CONS_GCF_2_TIM_R6 and GO_CONS_GCF_2_SPW_R4 were the best performers with standard errors of 0.1014, 0.1019 and 0.1022 m respectively. In terms of gravity anomalies, EGM2008, SGG-UGM-1 and EIGEN-6C produced the best fit because of their low standard errors of 8.149, 8.187 and 8.349 mGal, respectively.

The new GGM, which was named PM_com_1c, was computed by selecting from the best performing GGMs, the harmonic coefficients producing the largest signal to noise ratio of the disturbing potential. After comparison of PM_com_1c with the other GGMs, it was revealed that it produced larger cumulative signal to noise ratio in the disturbing potential, gravity anomaly and geoid undulation, than all the individual GGMs, in all parts of the harmonic spectrum. This study recommends the use of PM_com_1c or other regionally combined GGM for gravimetric geoid modelling in Peninsular

Malaysia. It is expected that, when such regional geopotential models are used to provide the long wavelength components of the gravity field, the quality of regional geoid models will improve.

References

[1] Ince E S, Barthelmes F, Reißland S, Elger K, Förste C, Flechtner F and Schuh H 2019 ICGEM-15 years of successful collection and distribution of global gravitational models, associated services and future plans *Earth Syst. Sci. Data Discuss.* 1–61
[2] Aziz; W, Fashir; H H and Zainon; O 1998 Evaluation of the EGM96 Model of the Geopotential In Peninsular Malaysia pp 1–16
[3] Pa'suya M F, Din A H M, McCubbine J C, Omar A H, Amin Z M and Yahaya N A Z 2019 Gravimetric Geoid Modelling Over Peninsular Malaysia Using Two Different Gridding Approaches for Combining Free Air Anomaly *ISPRS - Int. Arch. Photogramm. Remote Sens. Spat. Inf. Sci.* **XLII-4/W16** 515–22
[4] Rapp R H 1973 Geoid information by wavelength *Bull. Géodésique* **110** 405–11
[5] Pa'suya M F, Din A H M, Yusoff M Y M, Abbak R A and Hamden M H 2021 Refinement of gravimetric geoid model by incorporating terrestrial, marine, and airborne gravity using KTH method *Arab. J. Geosci.* **14** 2003
[6] Rapp R H 1974 Comparison of the potential coefficient models of the standard Earth (II and III) and the GEM 5 and GEM 6 279–87
[7] Bašić T, Denker H, Knudsen P, Solheim D and Torge W 1990 A New Geopotential Model Tailored to Gravity Data in Europe *IAG- General Meeting, 3-12 August 1989* (Edinburg, Scotland) pp 109–18
[8] Ågren J 2004 *Regional Geoid Determination Methods for the Era of Satellite Gravimetry: Numerical Investigations Using Synthetic Earth Gravity Models* (PhD, Dissertation, Royal Institute of Technology, Stolkholm, Sweden)
[9] Heiskanen W and Moritz H 1967 *Physical Geodesy* ed J Gilluly and A O Woodford (San Francisco and London: W H Freeman and Company)
[10] Torge W 2001 *Geodesy* (Berlin, New york: Walter de Gruyter)
[11] Gachari M K and Olliver J G 1986 The detailed gravimetric geoid of Kenya *Surv. Rev.* **28** 365–71
[12] Sideriss M G 2011 Geoid Determination , Theory and Principles *Encycl. Earth Sci. Ser.* **Part 5** 356–62
[13] Kirby J and Featherstone W 1997 A Study of Zero-and first-degree terms in geopotential models over Australia *Geomatics Res. Australas.* **66** 93–108
[14] Nyoka C J, Din A H M D and Pa'suya M F 2021 Computation of Gravity Field Functionals with a localized level Ellipsoid *J. Inf. Syst. Technol. Manag.* **6** 226–42
[15] Moritz H 1992 Geodetic reference system 1980 *Bull. Géodésique* **54** 395–405
[16] Mäkinen J 2021 The permanent tide and the International Height Reference Frame IHRF *J. Geod.* **95** 1–19
[17] Ekman M 1996 The permanent problem of the permanent tide : What to do with it in geodetic reference systems ? *Marees Terr.* **125** 9508–15
[18] Mäkinen J and Ihde J 2009 The Permanent Tide In Height Systems2 *Observing our Changing Earth* ed M G Sideris (Berlin, Heidelberg: Springer Berlin Heidelberg) pp 81–7
[19] Rapp R H, Nerem R S, Shum C K, Klosko S M and Williamson R G 1991 Consideration of permanent tidal deformation in the orbit determination and data analysis for the TOPEX/POSEIDON mission *NASA Tech. Memo. 100775* **1**
[20] Zhang P, Bao L, Guo D, Wu L, Li Q, Liu H, Xue Z and Li Z 2020 Estimation of vertical datum parameters using the gbvp approach based on the combined global geopotential models *Remote Sens.* **12** 1–23
[21] Din A H M, Abazu I C, Pa'Suya M F, Omar K M and Hamid A I A 2016 The impact of sea level

rise on geodetic vertical datum of Peninsular Malaysia *Int. Arch. Photogramm. Remote Sens. Spat. Inf. Sci. - ISPRS Arch.* **42** 237–45
[22] Hamden M H, Din A H M, Wijaya D D, Yusoff M Y M and Pa'suya M F 2021 Regional Mean Sea Surface and Mean Dynamic Topography Models Around Malaysian Seas Developed From 27 Years of Along-Track Multi-Mission Satellite Altimetry Data *Front. Earth Sci.* **9** 1–16
[23] Ekman M. 1989 Impacts of geodynamic phenomena on system for height and gravity *Bull. Géodésique* **63** 281–96
[24] Ustun A and Abbak R A 2010 On global and regional spectral evaluation of global geopotential models *J. Geophys. Eng.* **7** 369–79
[25] Tsoulis D, Zoi I, Georgios; P, Diamantis; K, Thomas; P, Konstantinos; P and Ioannis; V 2011 Spectral analysis and interpretation of current satellite-only Earth gravity models by incorporating global terrain and crustal data *ESA*
[26] Tziavos I N, Vergos G S, Grigoriadis V N, Tzanou E and Natsiopoulos D A 2015 Validation of GOCE/GRACE Satellite Only and Combined Global Geopotential Models Over Greece in the Frame of the GOCESeaComb Project *International Association of Geodesy Symposia* pp 145–53
[27] Ismail M K, Din A H M, Uti M N and Omar A H 2018 Establishment of new fitted geoid model in Universiti teknologi Malaysia *Int. Arch. Photogramm. Remote Sens. Spat. Inf. Sci. - ISPRS Arch.* **42** 27–33
[28] Kotsakis C and Sideris M G 1999 On the adjustment of combined GPS/levelling/geoid networks *J. Geod.* **73** 412–21
[29] Sjöberg L E and Bagherbandi M 2017 *Gravity Inversion and Integration: Theory and Applications in Geodesy and Geophysics* (Berlin: Springer International Publishing)
[30] Goyal R, Dikshit O and Balasubramania N 2018 Evaluation of global geopotential models: a case study for India *Surv. Rev.* 1–11
[31] Ghilani C D and Wolf P R 2006 *Adjustment Computations: Spatial Data Analysis* (John Wiley & Sons, Inc)
[32] Setan H and Singh R 2001 Deformation analysis of a geodetic monitoring network *Geomatica* **55** 333–46
[33] Marotta G S and Vidotti R M 2017 Development of a Local Geoid Model at the Federal District, Brazil, Patch by the Remove- Compute-Restore Technique, Following Helmert's Condensation Method *Bol. Ciencias Geod.* **23** 520–38
[34] Kumar M 1988 World geodetic system 1984: A modern and accurate global reference frame *Mar. Geod.* **12** 117–26
[35] Sánchez L and Sideris M G 2017 Vertical datum unification for the International Height Reference System (IHRS) *Geophys. J. Int.* **209** 570–86
[36] Jalal S J, Musa T A, Md Din A H, Wan Aris W A, Shen W Bin and Pa'suya M F 2019 Influencing factors on the accuracy of local geoid model *Geod. Geodyn.* **10** 439–45
[37] Kotsakis C and Katsambalos K 2010 Quality analysis of global geopotential models at 1542 GPS/levelling benchmarks over the Hellenic mainland *Surv. Rev.* **42** 327–44

Acknowledgement
The authors are very grateful to the Department of Survey and Mapping, Malaysia for supplying the GNSS-levelling and gravity data that was used in this study. This project is sponsored by the Ministry of Higher Education (MOHE) under the Fundamental Research Grant Scheme (FRGS) Fund, Reference Code: FRGS/1/2020/WAB07/UTM/02/3 (UTM Vote Number: R.J130000.7852.5F304).